Flexible graphene solution-gated field-effect transistors: An efficient transducer for µ-ECoGs

Authors: Clement Hebert[1], Eduard Masvidal-Codina[2,3], Alejandro Suarez-Perez[4], Andrea Bonaccini Calia[1], Gaelle Piret[5], Ramon Garcia-Cortadella[1], Xavi Illa[2,3], Elena Del Corro Garcia[1], Jose M De la Cruz Sanchez[1], Elisabet Prats-Alfonso[2,3], Jessica Bousquet[1], Philippe Godignon[2,3], Blaise Yvert[5], Rosa Villa[2,3], Maria V. Sanchez-Vives[4,6], Anton Guimerà-Brunet[2,3], Jose A. Garrido[1,6]

[1] Catalan Institute of Nanoscience and Nanotechnology (ICN2), CSIC and The Barcelona Institute of Science and Technology, Campus UAB, Bellaterra, 08193 Barcelona, Spain

[2] Instituto de Microelectrónica de Barcelona, IMB-CNM (CSIC), Esfera UAB, Bellaterra, Spain

[3] Centro de Investigación Biomédica en Red en Bioingeniería, Biomateriales y Nanomedicina (CIBER-BBN), Madrid, SPAIN

[4] Institut d'Investigacions Biomèdiques August Pi i Sunyer (IDIBAPS), Barcelona, Spain

[5] INSERM U1205, Grenoble, France

[6] ICREA, Pg. Lluís Companys 23, 08010 Barcelona, Spain

Corresponding authors: Clement Hebert, Jose A. Garrido

E-mail: clement.hebert@icn2.cat; joseantonio.garrido@icn2.cat

Keywords: *graphene, field-effect transistor, electrocorticography, neurotechnology, brain-computer interfaces.*

This is the peer reviewed version of the following article: Hébert C., Masvidal-Codina E., Suarez-Perez A., Calia A.B., Piret G., Garcia-Cortadella R., Illa X., Del Corro Garcia E., De la Cruz Sanchez J.M., Casals D.V., Prats-Alfonso E., Bousquet J., Godignon P., Yvert B., Villa R., Sanchez-Vives M.V., Guimerà-Brunet A., Garrido J.A. Flexible Graphene Solution-Gated Field-Effect Transistors: Efficient Transducers for Micro-Electrocorticography, which has been published in final form at https://doi.org/10.1002/adfm.201703976. This article may be used for non-commercial purposes in accordance with Wiley Terms and Conditions for Self-Archiving."

Abstract

Brain-computer interfaces and neural prostheses based on the detection of electrocorticography (ECoG) signals are rapidly growing fields of research. Several technologies are currently competing to be the first to reach the market; however, none of them fulfil yet all the requirements of the ideal interface with neurons. Thanks to its biocompatibility, low dimensionality, mechanical flexibility and electronic properties, graphene is one of the most promising material candidates for neural interfacing. After discussing the operation of graphene solution-gated field-effect transistors (SGFET) and characterizing their performance in saline solution, we report here that this technology is suitable for μ-ECoG recordings through the studies of spontaneous slow wave activity, sensory evoked responses on the visual and auditory cortices, and synchronous activity in a rat model of epilepsy. An in depth comparison of the signal-to-noise ratio of graphene SGFETs with that of platinum black electrodes confirms that graphene SGFET technology is approaching the performance of state-of-the art neural technologies.

Introduction

The progress of neural technologies over the last twenty years brings new hope for people with neural disorders or motor and sensory functional loss. Thanks to the development of new brain interfaces for both recording and stimulation, novel techniques are now available to control artificial limbs through brain computer interfaces (BCI) [1], and to alleviate the trembling in Parkinson's disease [2] or treat pharmaco-resistive depression by means of deep brain stimulation (DBS) [3]. Other preclinical studies have also reported promising results to restore locomotion in paraplegic rats [4] or to recruit healthy brain regions to perform new tasks for neural rehabilitation after brain injuries [5]. Most of these techniques rely on efficient electric neural interfaces for recording or stimulation. Electrical recordings of the brain have been performed for long using non-invasive electroencephalography (EEG). However, the spatial resolution offered by this technique is poor because of the skull's filtering and is not able to provide enough information to decipher neural signals with the precision required for an efficacious application of neural interfaces [6,7].

Neuroscientists and neurosurgeons are thus looking for technologies that could ideally record the whole brain with a high spatial and temporal resolution. Electrocorticography (ECoG) is the current clinical solution to obtaining brain recordings with high temporal resolution. ECoG consists in placing arrays of large-diameter electrodes (few millimeters) directly on the cortex. To overcome the spatial resolution issue, microelectrode arrays (MEAs) with electrode diameters ranging from 10 to 100 μm and electrode-to-electrode separation down to 30 μm have been developed, offering very good spatial and temporal resolutions [8]. MEAs opened a new field of ECoG called μ-ECoG, which is a very powerful technique

to investigate neural network function but also to establish novel diagnostic procedures, and will certainly be a major component for future neural prostheses[9,10]. Nevertheless the surface covered by the MEAs is limited due to the spatial constraints of the connections to the recording system [8]. Furthermore, covering an important part of the brain with the density of the MEAs would require hundreds of thousands of channels that cannot be acquired nor analysed in parallel with the currently available computing technologies. Emerging ideas thus suggest developing a mesoscale technology able to record on large surfaces with an intermediate spatial resolution [11],[12]. The goal is to record the low-frequency (below 500 Hz) signals coming from a large number of cortical columns that are separated by around 1 mm in the human brain.

In the last 10 years, significant efforts have been made to develop µ-ECoG technologies capable of providing good signal–to-noise ratios and high flexibility (reaching conformability and stretchability) with a strong emphasis on the materials used for the transducing elements of the neural interfaces[12],[13]. So far most of the electrode materials recently investigated are based on porous metals, oxides or conductive polymers. The current µ-ECoG technology offers arrays of transducing elements, electrodes or transistors, with up to 360 recording sites[12]. However, chronic studies of neural signals are still precluded by the electric recording interface; partly because the mismatch of the Young moduli and the chemical nature of the transducing material induce fast degradation of the quality of recorded signals. The substrate used for the scaffold of the implant also plays an important part in the efficiency of technology. The substrate must be very flexible, even more than the transducing material, to reach the conformability of the full device to the brain shape, highly biocompatible and highly stable. So far the most commonly used flexible substrates are parylene, polydimethylsiloxane (PDMS), polyimide and SU8[14]. Some other more advanced bio-inspired polymers are under investigation to improve the substrates' performance [15].

Thanks to their suitability for flexible technology and their high biocompatibility, graphene-based materials are considered as material platform with very high potential for neural interfaces[16–19]. Additionally, graphene exhibits extraordinary electrical properties such as high carrier mobility[20], chemical stability[21] and very good mechanical conformability[22], features that only few materials such as conductive polymers can offer [23]. This helps to create a very intimate interface between the tissue and the transducing system. Moreover, single layer graphene prepared by chemical vapour deposition (CVD) provides optical transparency[24]. This feature is very interesting for the study of neural networks and especially of cortical features where optogenetics and calcium imaging can provide complementary information[22,25]. Before graphene was tried for neural recording, only few materials such as indium tin oxide[26] or conductive polymers[27] offered the transparency required to combine optogenetics and electrical neural recordings.

Previous *in vivo* studies using single layer CVD graphene have used the electrode configuration; nonetheless, we propose here the use of a transistor configuration. The main reason for this choice is certainly the local pre-amplification that is inherent to the transistors configuration. As a consequence, no electronic amplification module needs to be added as close as possible to the recording site to minimize the environmental noise. Prior to graphene transistors, PEDOT:PSS (poly(3,4-ethylenedioxythiophene) doped with poly(styrene sulfonate) anions) transistors already proved that this type of active devices can provide very good performance for μ-ECoG[28]. They will be used here as a reference to benchmark the properties of the graphene transistors.

In this Feature Article we explain the fundamentals of the graphene solution-gated field-effect transistor and present a deep analysis of the performance of the flexible graphene transistors we have so far developed. A full description of the fabrication technology and of the custom characterization electronic system is also presented. The transistors are fully characterized in terms of transconductance and noise level in saline solution with an emphasis on the homogeneity of the performance. The devices are finally used in *in vivo* experiments in which the transconductance and noise are first characterized during slow wave activity followed by the recording of visual and auditory evoked activity as well as of synchronous activity in a rat model of epilepsy. The *in vivo* performance is compared to platinum black (Pt black) electrodes, in order to benchmark graphene transistors against highly porous materials. The results presented here are also compared to the available literature on graphene devices used for neural interfaces.

Graphene solution-gated field-effect transistor

a. Concept of the flexible graphene solution-gated field-effect transistor

The first solution-gated field-effect transistor was developed by Bergveld in 1970 using silicon[29]. The main difference between the working principle of a metal-oxide-semiconductor field-effect transistor (MOSFET) and the working principle of a SGFET is the way in which the current is modulated by the gate electrode. In a MOSFET, the current through the transistor is usually gated by a metal, which is separated from the channel by a thin insulating (oxide) layer. In a SGFET, on the other hand, the gate voltage is applied by a reference electrode immersed in an electrolyte. The possibility of using graphene in a solution-gated transistor configuration in aqueous medium is due to the special interface that is created between the graphene and a polarisable electrolyte. Electrochemical studies have shown that graphene behaves nearly as an ideal polarizable electrode[30],[31]; i.e. in an electrolyte without any redox species that could react under the electrochemical window of water (around 1.2 V), no charge is transferred across the interface[32]. Instead, ions accumulate at the surface of graphene when a potential is applied between a reference electrode and graphene. The graphene-electrolyte interface can be modelled as a series combination of two capacitors (Fig. 1a). The first component is the typical electrical double layer capacitance (EDLC), accounting for two layers of ions that are created at the surface of a

polarized electrode. The first layer is constituted of ions of opposite charges to those present in the electrode part, and the second layer is composed of ions of both positive and negative charges that progressively reach the potential of the solution far from the electrode. In addition, the quantum capacitance accounting for the variation of charge carriers induced by the change of the potential in the graphene layer must also be considered to fully model the graphene-electrolyte interface. In the case of graphene, the quantum capacitance is small near the charge neutrality point where the density of states is low [33]. Therefore, at low charge carrier densities, the quantum capacitance becomes lower than the EDLC and thus prevails in the interfacial capacitance (see figure 1).

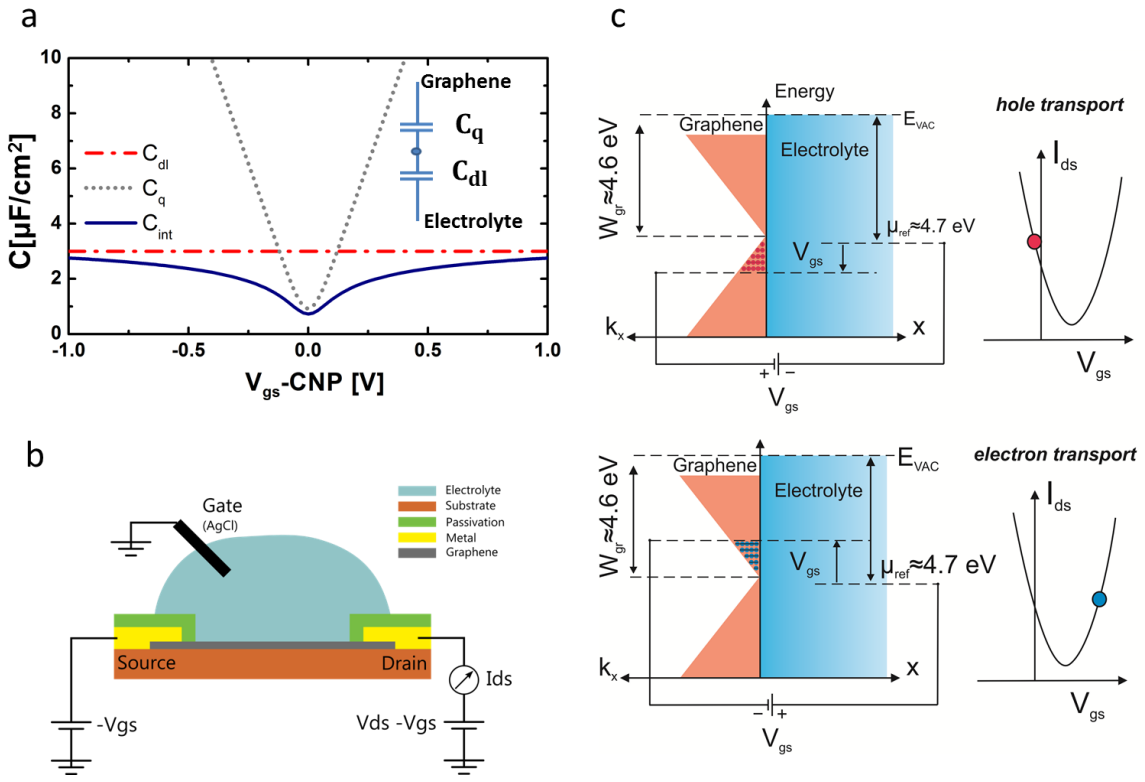

Figure 1: The graphene electrolyte interface and the concept of graphene solution-gated field-effect transistors. a) Simulation of the graphene-electrolyte capacitance at different polarizations. The interfacial capacitance (C_{int}) is the series combination of the double layer capacitance (C_{dl}) and the quantum capacitance (C_q). b) Cross section of the graphene solution-gated field-effect transistor device. The gate-source polarisation is applied on the gate and the drain source polarisation is applied on the drain. The drain source current I_{ds} is measured on the drain side. c) Simplified momentum-energy diagrams of the graphene-electrolyte interface in the case of the Ag/AgCl reference electrode (electrochemical potential, μ_{ref}, around 4.7eV) and their related drain-source current to voltage gate are shown. The work function of the graphene, $W_{gr,}$ is around 4.6eV. The electronic transport is governed by holes when the graphene electrode is positively biased and by electrons when negatively biased.

The graphene solution-gated field-effect transistor consists of a single layer graphene sheet, the channel, connected by two metallic contacts, namely the drain and the source, interfaced by an electrolyte in which a reference electrode (typically Ag/AgCl) is immersed to be used as the gate terminal that modulates the conductivity of the graphene sheet (Fig. 1b). A simplified version of the energy band diagram of the graphene electrolyte interface explains the modulation of the conductivity of the graphene sheet when sweeping the gate bias (Fig. 1c). It shows that by applying a voltage between the reference electrode and graphene, the Fermi level in graphene is shifted, consequently modulating the number of free carriers in graphene. The minimum of free carriers, and thus the minimum of conductivity, is reached when the valence and the conduction band meet at a point called the Dirac point; the gate bias potential at which the Fermi level reaches the Dirac point is the charge neutrality point (CNP). Depending on the position of the Fermi level with respect to the CNP, the transport in the graphene channel will be dominated by holes or electrons (Fig. 1c). Graphene transistors are thus ambipolar devices, a characteristic feature of its particular band diagram. The exact gate voltage corresponding to the CNP point depends on many factors such as the doping level of the graphene sheet (either from graphene-substrate interaction or due to microfabrication residues [34]), the electrochemical potential of the reference electrode, or the properties of the electrolyte solution such as pH or ionic strength. This capability has been exploited to demonstrate pH sensors using graphene SGFETs [35],[36].

The drain-source current I_{ds} flowing in the transistor's channel depends on the width-to-length ratio (W/L), the charge carrier mobility (μ), and the total charge carrier density (n), which is obtained by integrating along the graphene channel taking into account the voltage drop due to the graphene-metal contact resistance (R_c) (see Equation 1)[37]. At the same time, the charge carrier density has two terms: One is the gate-induced charge density that depends on both the total interfacial capacitance (C_{int}) and the gate-source voltage applied (V_{gs}) with respect to the CNP; the other term is the minimum carrier concentration (n_o) (Eq.2)[37], which finds its origin in substrate impurities and charge traps [15]. The efficiency of the modulation of the drain-source current by the gate voltage is given by the so-called transconductance (g_m), which is defined as the derivative of the I_{ds}-V_{gs} tranfer curve.

$$I_{ds} = \frac{W}{L}\mu \int_{I_{ds}\,R_c}^{V_{ds-}\,I_{ds}\,R_c} n\,(V)\,dV \qquad (1)$$

$$n(V) \approx \sqrt{{n_o}^2 + [C_{int}(V) \cdot \left[V_{gs} - V - CNP\right]/q\,]^2} \qquad (2)$$

The transconductance is thus proportional to the mobility of the graphene sheet and the interfacial capacitance. The values of carrier mobilities in graphene can reach theoretically up to 2 000 000

cm^2/Vs[38]. Experimentally, mobilities up to 140 000 cm^2/Vs at room temperature have been reported[39]. These values are far larger than in any other materials typically used for solution-gated field-effect transistors such as silicon, diamond or III/V semiconductors, which can hardly reach 3000 cm^2/Vs[40],[41] . Unlike standard field-effect technology, such as MOSFET technology, that uses a dieletric to create a capacitor, solution gating allows achieving a very high capacitance, leading to a very strong capacitive coupling. Actually, the thickness of the electrical double layer capacitor is extremelly thin so the electric field generated at the surface of the material is extremely high. It is thus possible to tune the number of carriers with lower applied gate bias than with a standard dielectric capacitor[42]. Even though solution gating is now widely used with ionic liquid to modulate the charge density in many semiconductors[43], only carbon materials such as graphene, diamond and carbon nanotubes (CNTs) are polarizable in acqueous electrolyte solution. In the case of graphene and diamond, the double layer capacitance is often reported to be about 2 $\mu F/cm^2$, which is one order of magnitude higher than for solution-gated transistors based on typical semiconductors. Indeed, for silicon or GaN, a passivation layer is required to avoid electron transfer with the solution, thus leading to a decrease in the electric field generated at their surface. Hence, the high values of interfacial capacitance and mobility allow graphene SGFET to have a very high transconductance, and thus high sensitivity to changes of the gate potential. Transconductance values of up to 4 mS/V (actually, this value corresponds to the transconductance normalized by the drain-source voltage) for a transistor of 20x10 μm^2 have been reported[44]. Moreover, such high transconductance allows to use drain-source bias voltages of graphene field-effect transistors in a narrow potential window below hundred millivolts. This feature is particularly important for neural interfaces because i) high applied potentials (above 1V) can have a significant influence on neural activity, and ii) low bias voltages result in low power consumption, a critical issue for chronic applications where the devices require an external battery.

b. The different kind of single layer graphene

As mentioned previously, the carrier mobility of graphene plays an important role in the performance of graphene SGFETs. The mobility is strongly affected by the crystal quality of the graphene; thus, the graphene quality and its preparation method is crucial to obtain very sensitive devices. The best performance of graphene is obtained using exfoliated graphene flakes. As previously mentioned carrier mobilities of up to 140 000 cm^2/V have been reported using exfoliated graphene[39]. However, exfoliated graphene cannot be seriously considered a source for commercial production of transistor arrays due to the poor up-scaling offered by this preparation technique. The most common method to obtain graphene with a fairly good quality over a large area is chemical vapour deposition. In the last decade big efforts have been done to develop high quality CVD graphene on a large scale. The growth of CVD graphene has been widely studied and developed in the industry using catalytic substrates (mainly copper) because these substrates offer the possibility to transfer the grown graphene layers onto other substrate. It is now possible, thanks to this technique, to produce and transfer graphene at a rather low cost over

30 inch wafers[45], or even squared meters[46]; mobilities superior to 2 000 cm^2/Vs can be regularly obtained on silicon dioxide substrates[47]. Higher mobilities, with values similar to those obtained with exfoliated graphene, have been reported for CVD graphene on hexagonal boron nitride (h-BN)[20].

c. Technology of flexible graphene field effect transistor

Various technology procedures have been reported for the fabrication of flexible transistors, but they all rely on very similar concepts (see Fig. 2). The first step consists in depositing a polymer, such as parylene, polyimide or SU8, on a silicon substrate. In order to ease the release of the device at the end of the fabrication process, a thin sacrificial aluminium layer could be deposited previous to the deposition of the polyimide[18]. The aluminium is chemically etched at the end of the process. Then the graphene is transferred from the growth substrate onto the polymer. To improve the resistivity of the contacts, the graphene can be transferred onto a substrate where the metallic tracks have already been defined. In order to define the shape of the transistor channel, the graphene is typically etched using oxygen plasma or reactive ion etching. A second metal layer for the contact is deposited and then insulated using a passivation layer, e.g. SU8 or polyimide. The quality of the graphene obtained on the growth substrate should not be affected by the technology process. For instance, it is very important to minimize any contamination of the graphene surface, such as the resist residues that are likely to remain after each photolithography step or after the transfer process of graphene. The impact of the transfer process is being discussed in the literature and is considered one of the limiting factors affecting graphene technology[48].

Figure 2b shows a photograph of a 4-inch wafer with 20 neural probes fabricated using the procedure described above. Figure 2c is a micrograph revealing the active area of a 4x4 array of graphene SGFETs, where one can notice the presence of circular perforations crossing the neural probes which main functions are to release the built-in stress during the fabrication procedures and to improve the adhesion of the probes to the cortex. Once the fabrication procedure is finalized the flexible probes are released from the silicon sacrificial wafer; Figure 2d shows an image of a released free standing neural probe (total thickness 10 µm) with its connector.

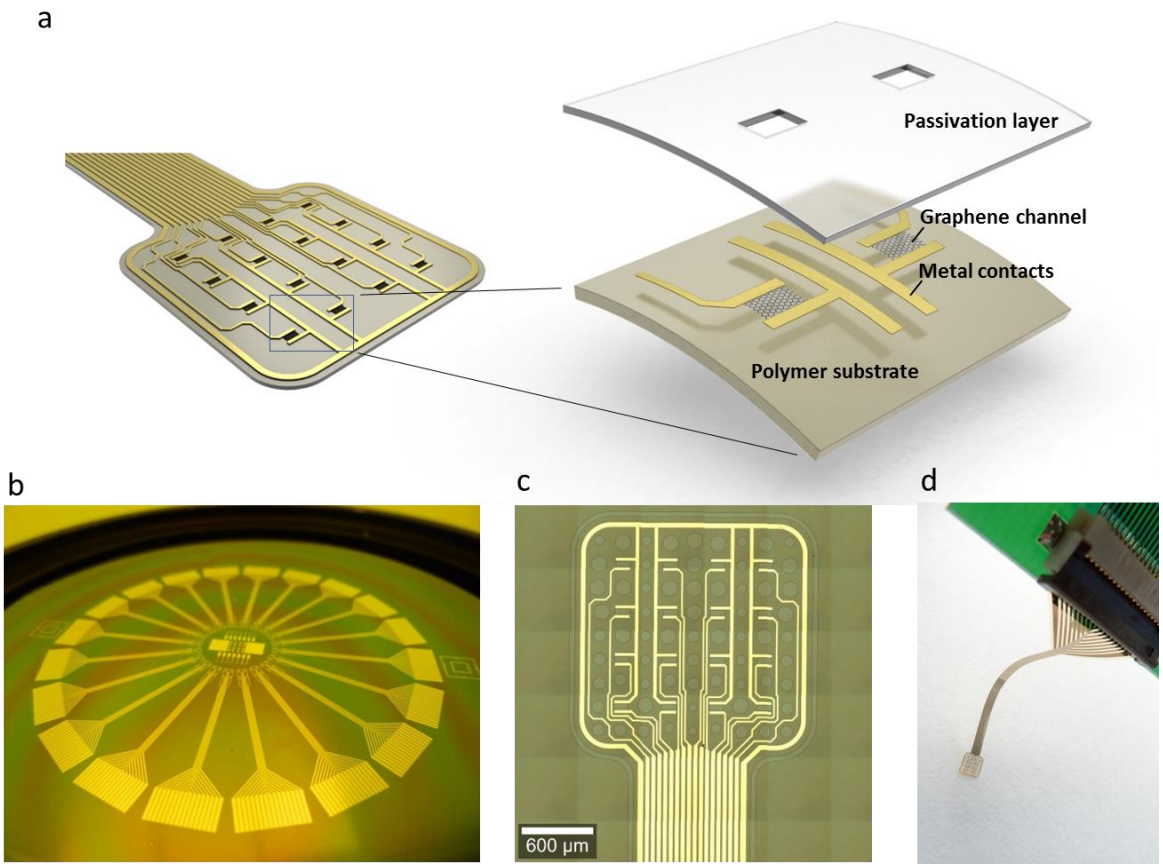

Figure 2: Technology of graphene SGFET arrays. a) Schematic of the graphene SGFET array. The explosive view shows the different components. b) Photograph of a 4-inch wafer containing 20 neural probes. c) Optical microscope picture of the active area of a 4x4 graphene SGFET array. d) Array of graphene SGFETs used for in vivo experiments connected to a zero insertion force connector.

d. Characterization of the flexible graphene field-effect transistors

Two standard sets of electrical characterizations are usually performed in saline solution to evaluate the performances of the transistors. We will refer to them as transistor transfer curve (I-V) characterization and noise characterization. In both cases, the experimental setup is the following. The probe is immersed in a buffered physiological-like solution, mostly phosphate buffered saline (PBS) or sodium chloride. An Ag/AgCl electrode is used as a reference. As mentioned previously, the position of the CNP depends on the pH and on the ionic concentration of the solution, so buffered solutions are preferred in order to keep the same pH from one measurement to another.

The I-V characterization consists in measuring the drain-source current I_{ds} for a fixed drain-source voltage V_{ds} as a function of the gate voltage V_{gs}. This characterization allows extracting the value of the transconductance g_m of the transistor and gives access to the value of the CNP. In this work the presented transconductance values are normalized by the applied V_{ds}, and the resulting units are [S/V]. These parameters help to evaluate the quality of the technology process. The typical transfer curves of a

graphene SGFET is sketched in figure 3a (solid black lines). There are several physical parameters such as the CNP, carrier mobility (μ), contact resistance (R_c) and minimum charge carrier concentration (n_o) that affect the transfer curve and transconductance (Fig. 3a). The CNP is strictly related to the doping of the graphene, and of course to the electrochemical potential of the used reference electrode. If the crystal is p-doped the CNP shifts to more positive values of V_{gs} and if it is n-doped to more negative values. The doping normally arises from post processing residues, as well as from charge traps in the substrate or from foreign atoms in the graphene lattice. The dotted line in Figure 3a represents the I-V curve a transistor with a p-type doping higher than that of the transistor represented by the solid line. The influence of mobility, contact resistance and minimum carrier density is shown in Figure 3a: the coloured areas correspond to simulations performed using a physical current-voltage model [37] in which one single parameter (μ, R_c, n_o) is varied between values higher and lower than that represented by the solid line. As can be seen, n_o and R_c have their main effect close to CNP or far from CNP, respectively. Furthermore, increasing R_c results in an increase of the non-linearity of the transistor curve. The mobility affects the overall shape of the transfer curve and has a strong impact on the maximum values of the transconductance.

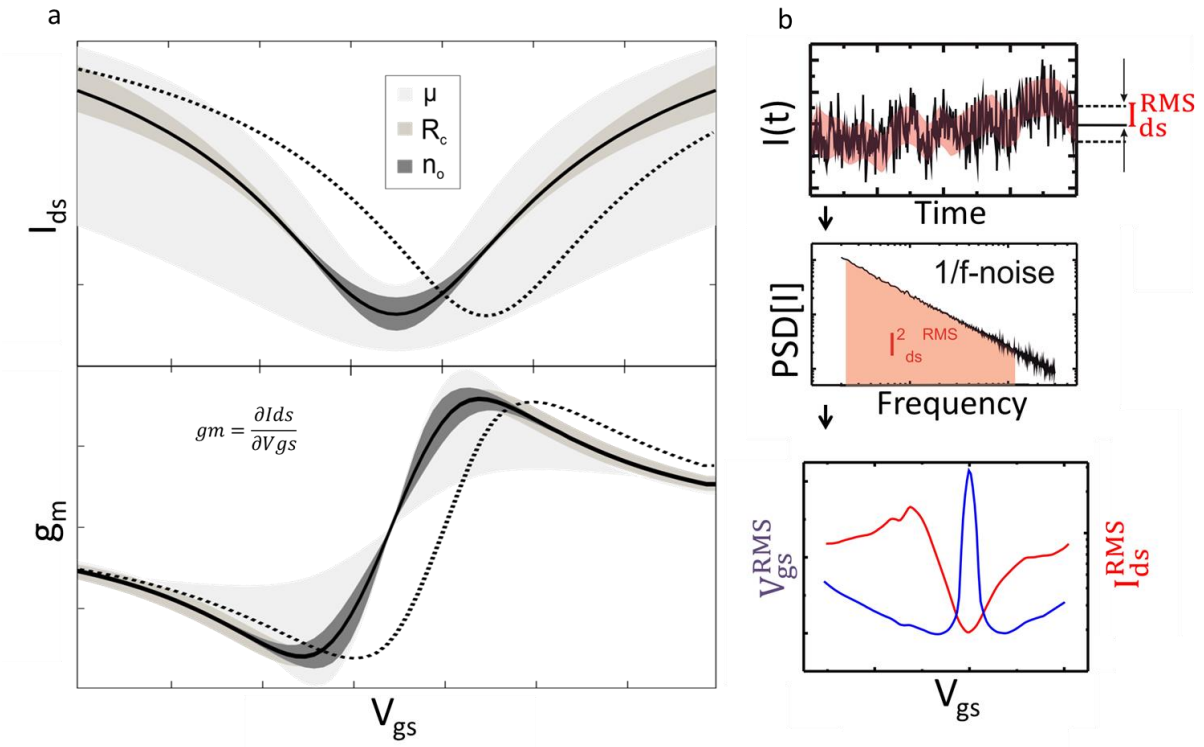

Figure 3: Standard characterization of graphene SGFETs in saline solution. a) Effect of mobility (μ), contact resistance (R_c) and minimum carrier concentration (n_o) on drain-source (I_{ds}) current and

transconductance (g_m) for different gate bias (V_{gs}). Dashed line indicates the shift induced by a change in the charge neutrality point (CNP). b) Measurement of the current fluctuation, determination of the power spectrum density (PSD) and the related root mean square (RMS) current noise and equivalent gate noise for different gate biases.

In order to characterize the electrical intrinsic noise of the device, the fluctuations of the I_{ds} are measured over time at fixed V_{ds} and V_{gs}. The fluctuations are then analyzed in the frequency domain and the power spectral density (PSD) of the current S_I is calculated (Fig. 3b). Graphene SGFETs exhibit 1/f noise, a type of noise also observed in other semiconductors and metals. The 1/f noise is fitted with $S_I = \frac{a}{f^b} I^2$ where *a* and *b* are the fitting parameters; typically, the *b* parameter is between 0.8 and 1.2 for graphene SGFETs. The *a* parameter corresponds to the amplitude of the low frequency noise at 1 Hz and is employed to understand the origin of the noise. A more useful noise figure of merit of the transistor as a sensor is the root mean square (RMS) drain-source current noise (I_{ds}^{RMS}), which can be extracted from the current PSD by integrating over the frequency bandwidth of interest. The equivalent effective gate voltage fluctuation (V_{gs}^{RMS}) is finally obtained by dividing I_{ds}^{RMS} by the transconductance. An example of typical curves of the equivalent gate voltage noise as a function of the gate voltage are presented in Figure 3b. The equivalent RMS gate voltage noise is the relevant figure of merit used to evaluate the ultimate recording resolution of the transistor.

Flexible graphene solution-gated field-effect transistors for µ-ECoG recordings

This section summarizes different studies demonstrating the use of graphene SGFETs to record neural activity from the cortex surface. Arrays of transistors of 80x30 µm^2 (equivalent to an electrode of 55 µm of diameter) and 100x50 µm^2 (equivalent to an electrode of 80 µm of diameter) were used in the study. The fabrication procedure of the arrays is described in the Methods section. Directly after fabrication, the devices are first characterized in PBS. To obtain the transistor transfer curve, the gate voltage was swept between -0.3V and 0.6V and the drain-source voltage was fixed at 100 mV. Figure 4 shows the I-V transistor curves of one 80x30-µm^2 transistor array with all the transistors functional (Fig. 4a). The SGFETs in the array exhibit a mean transconductance (normalized by the drain-source voltage) of 2.4 mS/V with a standard deviation of 0.25 mS/V and a maximum value of 3.1 mS/V (see Fig. 4b). The mean CNP is 0.31 V vs Ag/AgCl with a standard deviation of 0.01 V. The mean field-effect mobility extracted from the transconductance is 863 cm^2/Vs with a standard deviation of 92 cm^2/Vs. The in saline characterization reveals a good homogeneity of the graphene SGFET performance for a given array.

As the capacitor formed at the graphene-electrolyte interface is constituted of ions that have a low mobility, the amplitude of interfacial capacitance might strongly depend on the frequency that is applied

on the gate even for frequencies below 1 kHz. This would result in a decrease of the transconductance with the frequency. This information is very important for calibrating the signals recorded with the transistors and also to assess the transistor behaviour in the frequency range of neural activity. Therefore, transconductance spectroscopy (Fig. 4c), which is the evolution of the transconductance with the frequency of the signal applied on the gate, was performed using a protocol defined in the Methods section. The module of the transconductance is rather constant up to 10 kHz and its dependency with the gate voltage is consistent with the transistor transfer curve. Thus, the values obtained when measuring the transistor transfer curve can apply to the recording of higher frequency signals. The grey shadowed areas in the curve correspond to the bandwidth limited by the analog filters of our setup (between 0.1 Hz and 10 kHz). It is thus possible that graphene SGFETs can be operated at gate frequencies even higher than 10 kHz.

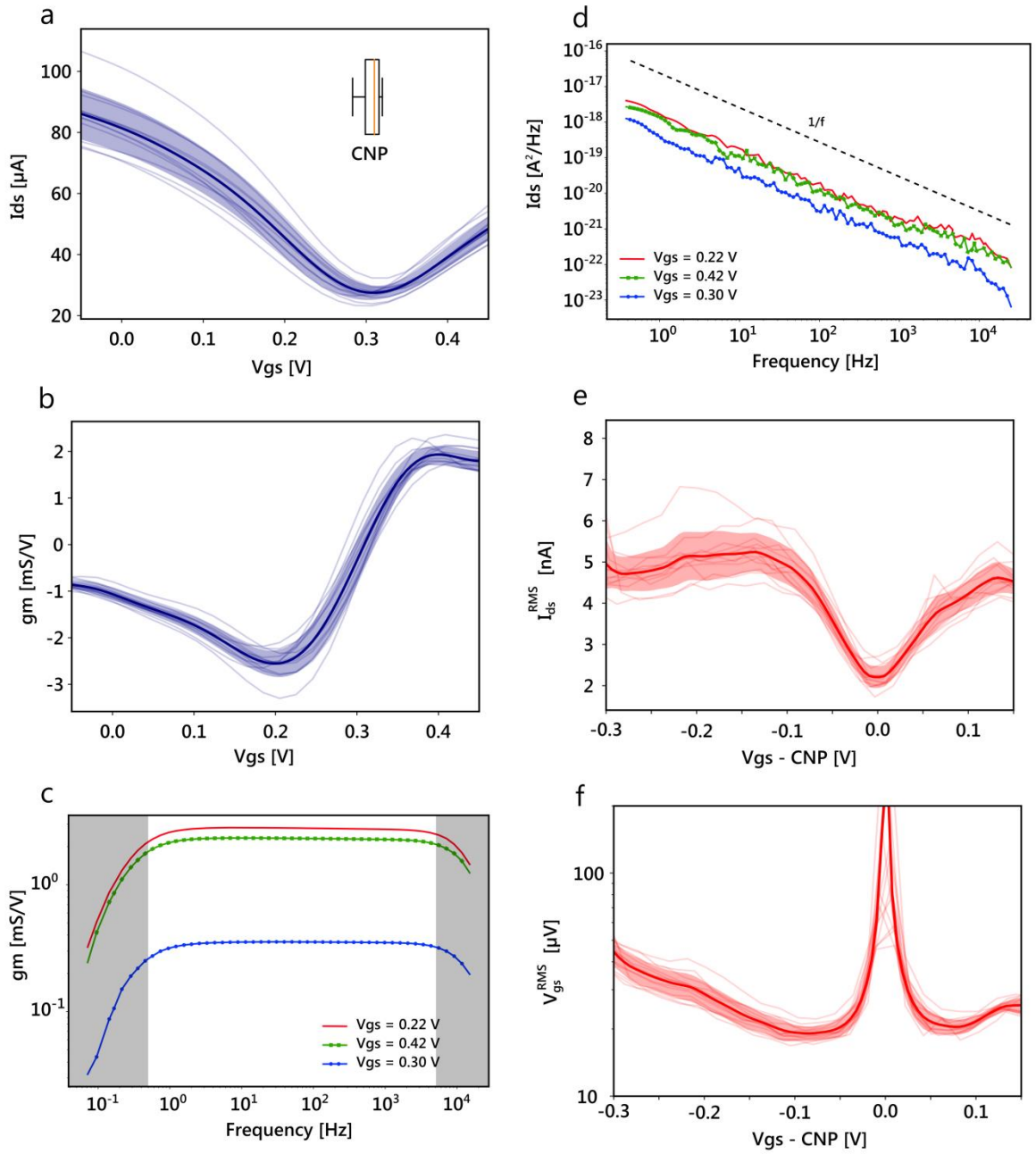

Figure 4: Characterization of the 80x30-µm^2 transistor array in PBS using V_{ds}=100mV. a) Transistor transfer curves. The insert shows the dispersion of the position of the charge neutrality point (CNP). b) Normalized transconductance curves of the transistors shown in part a. c) Normalized transconductance spectroscopy for various gate voltages. The response in the shadowed areas is dominated by the cutoff frequencies of the analog filters built in the recording equipment (see Methods section). d) Power spectral density of the drain source current for various gate voltages. e) RMS drain source current versus gate voltage. f) Equivalent RMS gate noise versus gate voltage.

Regarding noise, the mean equivalent gate noise is 21 μV RMS (integrated between 1Hz and 5kHz) with a standard deviation of 2 μV. A minimum value down to 18 μV RMS was obtained in the case of the 80x30 μm^2 arrays (Fig. 4d) and down to 15 μV in the case of the 100x50 μm^2 arrays.

Several experiments were conducted to evaluate the performance of graphene FET for recording μ-ECoGs. Platinum (Pt) black electrodes with a diameter of 50 μm were used together with the graphene SGFETs as a reference control. The transistor transfer curve (Fig. 5a) and the transconductance (Fig. 5b) were measured before all the *in vivo* recordings for selecting the optimum gate bias and for calibrating the recorded signals. Typically, the gate voltage is fixed at a value where the value of the transconductance is the highest; in the particular case of the experiment shown in Figure 5, the gate was fixed at 100 mV versus the used reference electrode and the drain-source voltage at 50 mV. The transistor array, together with the Pt electrode array, are placed on the surface of the cortex of the anesthetised rat to record the slow wave activity during anaesthesia, which is a pattern of spontaneous rhythmic activity that alternates between periods of neural firing (Up states) and periods of silence (Down sates) at a frequency around 1 Hz [49,50]. This low frequency signal results from a synchronized state of the cortex and leads to high amplitude activity originating in neural assemblies; this well-studied, spontaneous activity pattern is consequently a convenient scheme to assess the performance of recording devices.

As shown in Figure 5c, graphene SGFETs are able to detect the slow wave activity with a similar amplitude to the one detected by Pt black electrodes. In order to further investigate the performance of the two sensors, the PSD of the Up and Down states recorded with the transistor array of 100x50 μm^2 and with the Pt black electrodes are calculated and plotted in Figure 5e. The signal-to-noise ratio over frequency can be extracted (Fig. 5f) from the PSD (power spectral density) using a procedure described in the Methods section[51]. In this particular case, graphene transistors exhibit a better performance than Pt black electrodes below 5 Hz. Between 5 Hz and 100 Hz, graphene transistors present a SNR as good as or slightly lower than the electrodes. Above 100 Hz, the SNR of the transistors becomes lower than that of the Pt black electrodes. This frequency analysis also shows that graphene transistors can measure signals up to nearly 1 kHz.

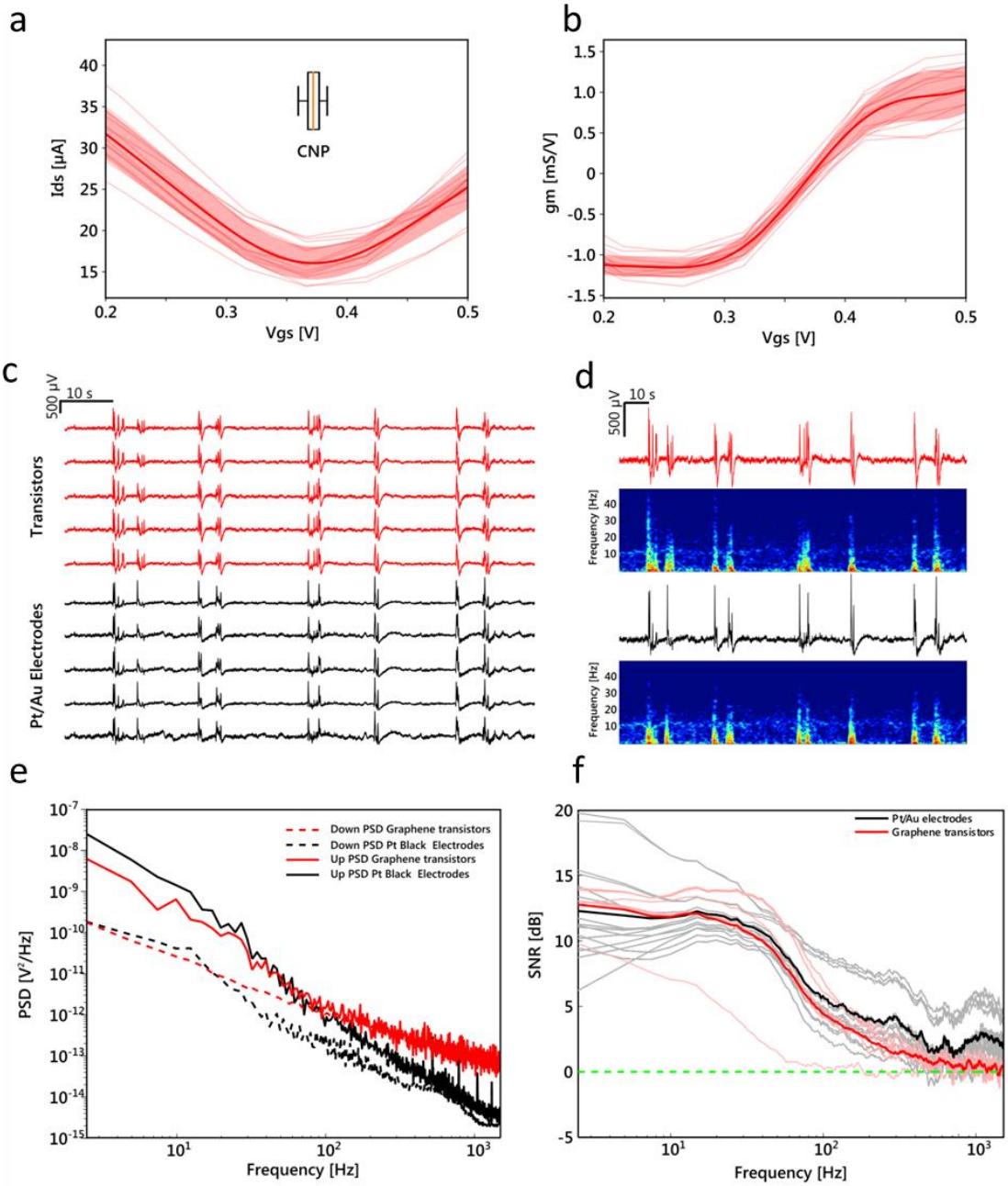

Figure 5: Recording of slow wave activity with graphene SGFET and comparison with platinum black electrodes. Recordings were obtained from the cerebral cortex in Wistar rats. a) *In vivo* transistor transfer curves using V_{ds} = 50mV. The insert shows the dispersion of the position of the charge neutrality point (CNP). b) Normalized transconductance versus gate noise for the devices shown in part a. c-f, recordings with graphene SGFET (red line) and platinum black electrodes (black line). c) Spontaneous oscillatory activity. d) Spectrograms of the spontaneous oscillatory activity. e) Power spectral density of the Up states (solid line) and Down States (dash line). f) Signal-to-noise ratio versus frequency extracted from the PSD for graphene SGFETs (light red lines) and platinum black electrodes (grey lines). The mean values are given by the bold lines.

To further assess the use of the flexible graphene transistors for future μ-ECoG clinical applications such as epilepsy diagnosis before surgical intervention, the WAG rat model of epilepsy [52,53] was used. Synchronous activity of WAG rats was recorded using the transistor array of 80x30 μm^2: 11 out of 12 transistors of the array can successfully record brain activity (Fig. 6a). The time-frequency analysis of the synchronous activity shows 3 - 4 Hz oscillations (Fig 6b).

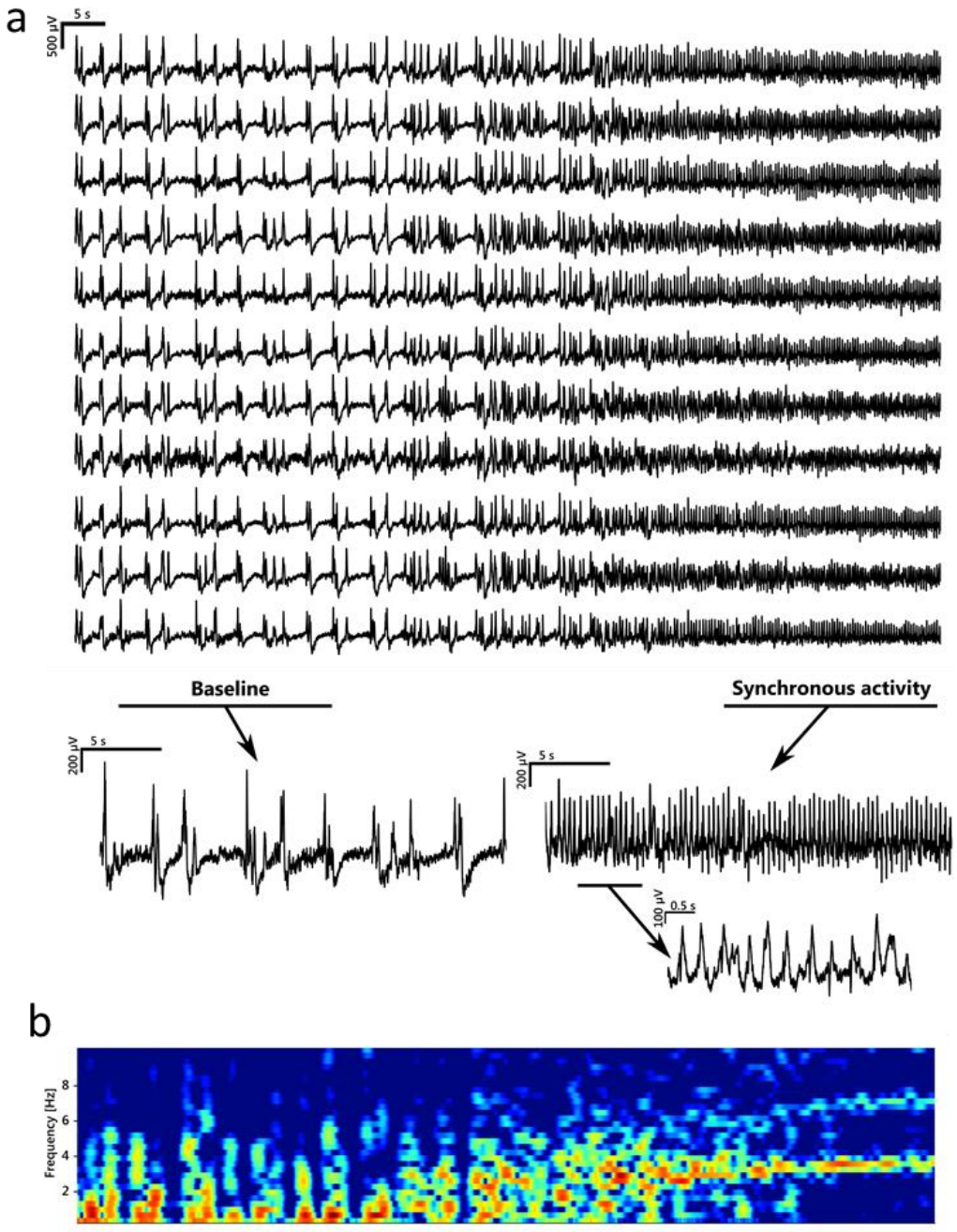

Figure 6. Synchronous activity recorded from the cerebral cortex of the WAG rat model of epilepsy. a) Simultaneous local field potential (LFP) recordings with an array of 11 working transistors. Towards the center of the recording, a synchronous activity characterized by a 3 – 4 Hz frequency starts. b) Spectrogram of one representative channel. Notice the 3 - 4 Hz discharge towards to last third of the

displayed recording Sensory evoked responses were also analysed to explore neural network activity given that they constitute a critical signal for the design of neural prostheses.

A good neural interface should be able to detect the evoked activity after one or few trials. To evaluate the potential of graphene transistors for possible applications involving sensory-evoked responses, visual and auditory evoked activity was investigated in each respective primary cortical region. Visual activity was evoked using a light stimulus provided by a white LED. An On-Off visually evoked-response occurred 40 ms after the stimulus and could be detected already after one single stimulus (Fig. 7a). The signal shows a main component with a frequency around 20 Hz with maximum amplitude of 250 µV and that lasts 70 ms.

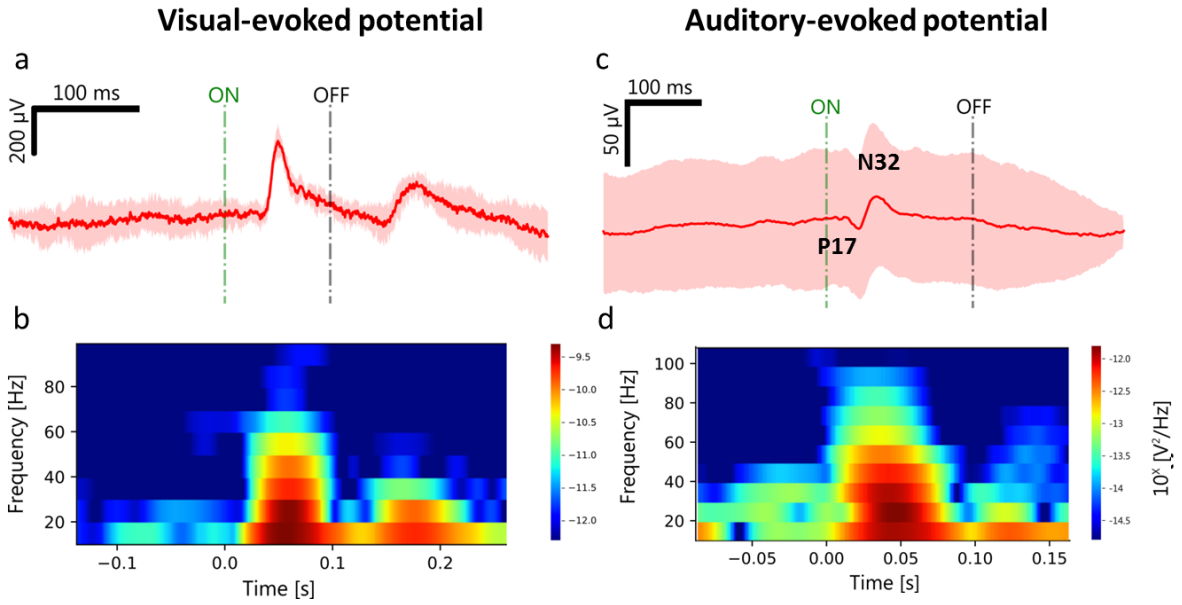

Figure 7: Sensory evoked potentials. Recordings were obtained from the primary visual (a,b) and primary auditory (c,d) cortices of Wistar rats during sensory stimulation protocols. a) Visual evoked potential (the dark red curve is the mean value of 10 events and the light red shadow represents the standard deviation). b) Spectrogram of visual evoked potential. c) Auditory evoked potential (the dark red curve is the mean value of 74 events and the light red shadow represents the standard deviation). d) Spectrogram of visual evoked potential.

Similarly, the graphene flexible implants with 80x30 µm^2 transistors were placed on top of the auditory cortex to record the evoked activity induced by sound following the protocol described in the methods section. A typical signal composed of two waves (P17 and N32) occurring around 10 ms after the stimulation could be detected (Fig. 7c) [51]. The signal shows a main component with a frequency around 25 Hz with a maximum amplitude of 15 µV and that lasts around 45 ms (Fig 7d). The low amplitude of

the signal is partly due to the background noise but might also indicate that the probe was not placed close enough to the area responding to the 8 kHz stimulus.

Discussion

Graphene-based devices using an electrode configuration have already been used to suggest that graphene is an interesting material platform for neural recordings[22,54]. In this Feature Article, we present and evaluate the performance of graphene SGFETs for the recording of several types of μ-ECoG signals. Hence, spontaneous slow wave activity during anaesthesia, synchronous activity in WAG rats and evoked visual and auditory potentials were studied using graphene SGFETs. These types of signals are very important for brain activity mapping, for the understanding of behavioural studies and for the development of neural prostheses. Recordings with graphene transistors have been benchmarked against the recordings obtained with Pt black electrodes.

The characterizations in PBS showed that the normalized transconductance of graphene transistors is around 3 mS/V, which is similar to the reported performance of organic electrochemical transistors (OECTs) based on PEDOT:PSS[55]; a direct comparison between these two devices might not be correct, since both type of transistors are based on different physical principles. The technology presented in this work results in graphene SGFETs exhibiting very homogenous transconductance and doping levels, which is important for the transistors to work at their best performances since only one gate potential can be applied to all the transistors. Moreover, the transconductance of graphene SGFETs was found to be constant up to at least 10 kHz, while PEDOT-based OECTs show a cutoff frequency of around 1 kHz [55]. It is worth mentioning that the cutoff frequency reported in our work is limited by the analog filters built in the custom recording electronic system (see Methods section).

In neural recordings, the intrinsic noise of the recording devices is one of the most relevant figures of merit. Even though local field potentials are signals with a rather large amplitude (above 70 μV) compared to spikes (10-20 μV), the recording device should offer an intrinsic noise level far below this value to achieve a high signal-to-noise ratio. The typical minimum RMS equivalent gate noise (frequency range between 1 Hz and 5 kHz) obtained with our flexible graphene transistor technology is between 18 μV and 23 μV for the 80x30 μm^2 array design and around 10 μV for the 100x50 μm^2 design. These values are in the range of or slightly above the ones commonly reported in the litterature for *in vitro* graphene SGFET. However, these values are still lower than the ones reported for doped graphene electrodes of 50x50 μm^2 (40 μV) thus showing a first advantage of transistor over electrodes [22]. The origin of the noise in graphene SGFETs is an active field of research and different sources of noise have been suggested. First, noise sources could be associated to the graphene quality. Single layer graphene layer presenting too many defects or second nucleation areas will result in electronic devices

with large noise because of charge scattering processes [56–58] . Second, it has been shown that the coupling between the graphene layer and the substrate can influence the electronic noise of the device: reports on the use of h-BN as a substrate for graphene or suspended graphene showed a significant improvement in the noise performance, which has been tentatively attributed to a reduction of interfacial traps and the roughness of the substrate [59]. In our study the value of the field-effect mobility of our graphene SGFETS on polyimide substrates is below 1000 cm^2/Vs, rather low compared to that obtained for graphene SGFETs prepared on silicon dioxide substrates using the same graphene quality which is around 2500 cm^2/Vs. Thus, the polyimide substrate might thus contribute significantly to the electronic noise of our devices. Finally, the contact resistance can be an important source of noise [60]: achieving very low contact resistance with 2D materials is indeed very challenging[61] , but we believe that it is a prerequisite for the development of low noise devices.

The flexibility of graphene SGFETs is one of their most interesting features for *in vivo* neural interfaces. Several strategies to assess the behaviour of the graphene transistor under stress can be explored. In order to investigate the stability of the flexible devices it is important to evaluate the impact of the bending on the performance of the transistors. Recently, our team has measured the transistor transfer curves when the transistor array is bent in a concave or a convex way[44]. We could show that the transistor transfer curves of flexible SGFETs remain the same as that of the flat array configuration when the devices are bent in concave and convex configurations, confirming that the devices performance is not affected by the curvature (bending radii was 10 mm). Going a step further, some studies have reported the use of graphene kirigami to achieve extremely flexible and stretchable SGFETs. In their studies, the authors show that even with a strain of 240% no change in the transconductance can be observed[62]. This structure has never been reported in an array configuration for µ-ECoG recording. However, this suggests that the graphene SGFET can be extremely folded to fit the shape of the brain gyri and sulci. This would help to have the device very close to the region of interest. On top of that, this extreme flexibility might provide tremendous advantages for surgical procedures in which the full device could be injected with a syringe like the neural electrode web developed by Lieber et al[63].

When placed on the cerebral cortex, graphene transistors exhibit similar performance (transconductance of 1 mS/V) as in PBS even though the gate is placed directly on top of the cortex. This indicates that the conductance of the neural tissue is sufficient to ensure a good modulation of the graphene channel. For the in vivo experiments described here, the drain-source voltage was fixed at 50 mV, leading to typical drain-source currents of 25 µA. The input power is thus around 1.25 µW for a single transistor. Given that the channel resistance is around 1 kΩ, this results in a local heating power of 0.625 µW. The gate voltage was fixed at around 100 mV where the transconductance was found to be the highest on the transistor curve. This gating voltage was found to be even closer to 0 V in a previous report[18]. Such low bias values are interesting not only to avoid local changes in neural activity but also for lower power

consumption. In comparison, PEDOT:PSS OECTs are reported to be biased with -400 mV for the drain-source voltage and a gate voltage of 300 mV, leading to a drain-source current of 200 μA[28]. The input power of the PEDOT:PSS transistors is thus around 80 μW, almost two orders of magnitude higher than that of the graphene SGFETs we report here. A low input power is of utmost importance, in terms of thermal dissipation and power consumption, to ensure the scalability of transistor arrays in which hundreds of recording transistors will be operating simultaneously.

During the recording of neural activity, we have demonstrated that flexible graphene SGFETs have a good capability for the detection of local field potentials, attested by the clear recordings of slow wave activity (see Figure 5). The signal-to-noise ratio of graphene SGFETs is similar to the SNR of platinum black electrodes, in particular for frequencies under 100 Hz. It is worth to notice that graphene SGFETs exhibit better performance than Pt black electrodes for very low frequency signals. This feature can be very interesting for studying very low frequency processes such as spreading depression[64]. The graphene SGFETs present a limit of detection at around 1 kHz, as shown in Figure 5f. This limit is fully sufficient for the recording of local field potential as well as multiunit activities above 200Hz.

Furthermore, we show here that graphene transistors can also be used for studying neural networks as well as for clinical diagnosis. The recordings of synchronous activity from the surface of the cortex discussed in this work are very clear, suggesting that graphene field-effect transistors can be used as a tool for detecting epileptic foci. Similarly, auditory and visual sensory-evoked potentials can be clearly distinguished after an average of 10 to 74 events and can thus be used for cortical mapping. In the case of the visual evoked potential, a single event is sufficient to detect the signal thus allowing on-line treatment of the information using recognition pattern algorithms for neural prostheses [65–67].

Graphene is the first atomically thin material able to detect such signals. This means that the challenge to achieve very low invasive devices relies now more on the development of the substrates or the surgery of implantation than on the sensing device itself. Thanks to the relatively good integration of graphene on any kind of substrate it would be possible to incorporate graphene SGFETs in transparent, extremely thin, flexible and stretchable substrates for spinal cord regeneration or intracortical recording, applications where the thickness and the rigidity of the devices should be as low as possible.

The next generation of graphene transistors might benefit greatly from the development of other 2D materials such as h-BN. Actually, carrier mobilities of up to 50 000 cm^2/Vs at room have been reported with CVD graphene on h-BN[20]. This will certainly help increase the sensitivity and decrease the power consumption of graphene transistors. Furthermore, h-BN substrate has also been shown to help reduce the noise of the graphene transistors[59]. If noise levels close to 1 μV are reached, it will be possible to record not only the multiunit activity at the surface of the cortex but also spiking activity once the transistors are used in penetrating configurations. This would open the path to simultaneous detection of surface local field potentials and deeper structure spike detection using graphene FETs.

An additional characteristic of the transistor configuration of graphene SGFETs is that they could potentially pave the way for chronic implants containing a very large number of recording sites. The current state-of-the art technology for clinical recording of the activity of epileptic foci is based on 30 to 256 electrodes[68–70]. This implies that up to 256 wires have to go from the brain to the recording systems. One of the solutions to overcome this issue is to use multiplexed electrode arrays, which would allow to reduce the number of connections from n^2 (non multiplexed nxn array) to 2n+1(multiplexed nxn array). Being two-terminal active devices, transistors offer advantages over electrodes for the design and implementation of multiplexed arrays. Indeed, the design of a multiplexed array of electrodes implies a higher level of complexity because it typically requires a buffer transistor connected to the electrode [12], which is not necessary in the case of the transistor configuration. Multiplexed technology is expected to be necessary for the development of chronic implants on large surfaces with a fairly high density of recording sites.

Conclusion

In this Feature Article we have discussed the current status of our technology for flexible graphene solution-gated field-effect transistor arrays. We have shown that transistor arrays fabricated on polyimide 4-inch wafers can be obtained with high homogeneity in terms of transconductance and position of the charge neutrality point, which reflects the quality of the CVD graphene layer as well as the relatively good maturity of the technology process. The intrinsic gate noise level of these transistors is around 20 μV rms, which is far below the amplitude of the local field potential than can be recorded at the surface of the cortex. *In vivo*, when placed on the surface of cortex for the recording of neural activity, graphene transistors exhibited signal-to-noise ratio similar to platinum black electrodes in the frequency range below 100 Hz and showed a recording limit for signals above 1kHz. Successful recordings of slow wave activity, synchronous activity and evoked potentials on the auditory and visual cortices have been demonstrated with flexible arrays of graphene SGFETs. Even at this early stage of development, graphene solution-gated field-effect transistor arrays already fulfil most of the requirement for μ-ECoG recordings. Additional improvement in implant design technology and combination with other 2D materials can now be tested to further improve this technology. Finally, we show that graphene SGFET exhibit similar performance than PEDOT:PSS OECTs, which are currently considered the state-of-the art flexible transistor technology for neural recordings. Graphene SGFETs provide significant advantage over PEDOT:PSS-based OECTs when considering the gate frequency response as well as power consumption. Compared to the graphene electrodes reported for μ-ECoG, additionally to the local amplification of the transistor—which is a clear advantage upon the electrode technology—, graphene SGFET exhibit lower noise and offer the possibility to develop multiplexing technology with a lower level of complexity. Considering that graphene SGFETs combine flexibility,

even stretchability if built in a proper design, biocompatibility and excellent neural recording performance, we believe that graphene SGFETs represent a very powerful technology that can help to advance the current knowledge and technology boundaries of *in vivo* neural electrophysiology.

Materials and Methods

Graphene CVD growth and transfer

Graphene was grown by chemical vapour deposition on a 4.5x7 cm^2 copper foil (Alfa Aesar Coated). Prior to the growth, the copper foil is electropolished during 5 min at fixed current density of 62 µA/cmin a solution containing H_20 (1 L) + H_3PO_4 (0.5 L) + ethanol (0.5 L) + isopropanol (0.1 L) and urea (10 g)[71]. Then the copper foil is loaded in a planar quartz tube (1600x60 mm) heated by a three zone oven. A first annealing step at 1015ºC under a 400 sccm Argon flow at 100 mbar during 1 h is followed by a 15-min growth step at 12 mbar under a gas mix of 1000 sccm Argon, 200 sccm hydrogen and 2 sccm methane.

A wet chemical method is used to transfer the graphene from the copper foil to the polyimide. First, a poly(methyl methacrylate) PMMA A2 is deposited on the graphene / copper foil and is let dry for 12 h. Subsequently, the back side graphene is etched. To achieve this, the sample is laid at the surface of an etchant solution composed of $FeCl_3$ / HCl (0.5M / 2M) for 2 min. The back of the sample side is then flushed with water. This operation is repeated at least three times to be sure that no residuals remain. The sample is laid on the etchant solution to remove the copper for at least 6h. Then the sample is cleaned several time in water and transferred onto the polyimide wafer previously activated by oxygen plasma. The wafer is dried for 30 min at 40ºC on a hot plate and then gradually up to 180ºC annealed in a vacuum oven. Finally the PMMA is dissolved in acetone and isopropanol.

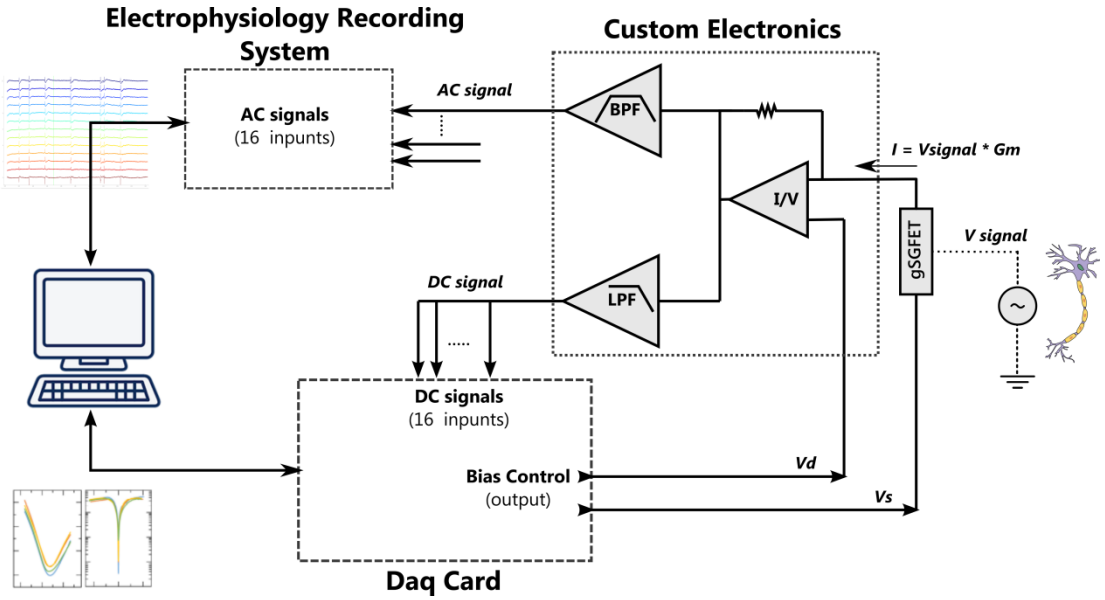

Figure 8: Schematic of the custom characterization setup used to interface commercial neural recording systems with the arrays of graphene SGFETs.

Custom characterization set up.

The commercially available electronics for recording electrophysiological signals has been commonly based on low noise voltage amplifiers, which amplify directly the signal provided by the electrodes. The developed SGFETs are not passive devices like the electrodes. SGFETs are active devices that provide local amplification by converting the input voltage signal into a current signal. Therefore, to make the SGFETs technology compatible with the commonly used recording systems a different input stage is required. Figure 8 shows the experimental setup used to perform the *in vivo* recordings. It is based on custom electronics that provide the current-to-voltage conversion and the bias control for each channel (up to 16 channels). It also splits the converted signals into DC (frequency < 0.1HZ) and AC (0.1 Hz < frequency > 5 kHz) components. Then, the AC signals can be directly acquired by a commercial electrophysiological recording system while the DC signals and bias control are managed by a data acquisition system (National Instruments USB-6353). The flexible samples are connected to our home made electronics via a 16-contact zero insertion force (ZIF) connector.

To perform the devices characterization both signals DC and AC are manged by the data acquisition system (National Instruments USB-6353). The transconductance spectroscopy is obtained by applying a signal in the reference gate electrode. This signal contains several harmonics in the frequency range of study. Then, the AC acquired signal is demodulated to obtain the transconductance for each evaluated frequency.

Device fabrication

A 10 µm thick biocompatible polyimide (PI) 2611 layer (HD MicroSystems) was spin-coated on a Si/SiO_2 wafer and cured under nitrogen atmosphere at 350ºC [72,73]. The first layer of Ti/Au (10 nm/100 nm) metal contacts are deposited by electron-beam vapour deposition and then structured in terms of optical lithography. Afterwards, CVD graphene is transferred to the wafer using a PMMA wet etching process as described in the previous section. The graphene active area W x L= 80x30 μm^2 or 100x50 μm^2 of the sensors is then defined by oxygen plasma in a reactive ion etching system (RIE). A second metallization layer of Ni/Au (20 nm/200 nm) is then evaporated and lithographically defined followed by a lift-off step. In order to avoid damaging the graphene with the ultrasounds of the sonicator, the lift-off is achieved by leaving the wafer 1 h in acetone and by flushing acetone with a syringe. Ni was chosen as the top source-drain contact for our graphene devices as it is one of the metals that forms strong chemical bonds with graphene through orbital hybridization, and more importantly, Ni appears

to provide the low contact resistance to graphene [74,75]. At this point the samples are then thermally annealed at 290ºC in ultra-high vacuum. To electrically insulate the device, a 2-µm-thick SU-8 epoxy photoresist (SU-8 2005 Microchem) layer is spin-coated and defined in such a way that only the graphene area is left uncovered.

Finally, the PI probes are cut by reactive ion etching using a protective Aluminum mask with the shape of the implants. To do so, the wafer is spin coated with a resist in order to protect the graphene. On top of the resist, a 500 nm-thick Al layer is sputtered and structured by photolitography and wet etching. Then the wafer is placed in the RIE system where the polyimide is cut in the unprotected regions. Once the PI is cut down to the Si/SiO2 substrate the Al is removed completely by wet etching and the resist with acetone and isopropanol.

The flexible PI implant with the graphene sensors are then peeled and released from the sacrificial Si/SiO2 wafer.

Animal and surgery procedure for slow oscillation and visual evoked potential recordings

For the *in vivo* experiments, adult male Wistar (n=15; 225-418g) and WAG (Wistar Albino Glaxo; n=4; 137-265g) rats from Charles River Laboratories International, Inc. were used. All experiments were supervised and approved by the university committee and were carried out in accordance with the present laws of animal care, EU guidelines on protection of vertebrates used for experimentation (Strasbourg 3/18/1986) and the local law of animal care established by the Generalitat of Catalonia (Decree 214/97, 20 July). The animals were placed in an anesthesia induction chamber for 5 minutes at 100% of O_2. Next, anesthesia was induced by raising the isoflurane concentration to 5% (0.6 L/min, 1 bar) for 5 more minutes always watching out respiration. We next set the concentration of isoflurane to 3% for one more minute before the rat was placed in the stereotaxic apparatus with mask delivering isoflurane and oxygen. For the rest of the surgery, 1.5-2% of isoflurane was used to maintain deep anesthesia. Heart rate was continuously monitored and maintained at ca. 300 bpm. A subcutaneous injection of atropine (0.05 mg/kg) was given to prevent respiratory secretions. All pressure points and tissues to be incised were sprayed with lidocaine before surgery. Body temperature was maintained at 37ºC. A craniotomy of 4 mm ML and 5 mm AP was performed in the left hemisphere revealing different cortical areas such motor (M1), somatosensory (S1) and visual primary (V1) cortices. Electrode recordings were pre-amplified with a multichannel system (Multichannel Systems, Germany) while graphene SGFET recordings were treated and pre-amplified with an electronic system developed by CNM (Centro Nacional de Microelectronica,

in Barcelona). The electronic system, controlled by MATLAB® 2014, consists in a 32-channel current-to-voltage converter Printer Circuit Board (PCB). Both were digitized at 10 KHz with a CED 1401 acquisition board and Spike2 software (Cambridge Electronic Design, UK). At the end of the experiments the animals were administered a lethal dose of sodium pentobarbital.

Slow oscillations recordings and SNR analysis

Spontaneous Slow Oscillations were recorded simultaneously using graphene SGFET probes and black platinum MEAs covering different areas of the cerebral cortex (S1, M1, V1). Signal analysis was performed using MATLAB® 2012a (The MathWorks Inc., Natick, MA). From the raw signal, Up and Down state detection was performed by using a reconstruction of the signal based on the principal component analysis (PCA) of three resulting signals obtained from applying different filters to the raw signal: smoothing filter with a 5-ms moving window, bandpass filter from 15 to 100 Hz[76], and MUA bandpass filter from 200 to 1500 Hz[77]. A threshold was set on the reconstructed signal to classify the parts of the recording with more frequency content (Up states) and less frequency content (Down states). For electrodes where the detection did not work, we used the detection times from the nearest electrode.

Once the detection was performed, the PSD with a resolution of 4096 points of the fast Fourier transform (FFT) was calculated for every Up and Down state separately using Welch's method. The mean PSD of the Up states and Down states in the recording fragment were calculated. The Spectral SNR was calculated for every transistor and electrode recording dividing the PSD (power spectral density) of Up states by the PSD of Down states and expressed it in decibels (dB).

Visual evoked response in *in vivo* recordings

Black platinum MEA and a graphene SGFET array were placed very close to each other primary visual cortex (V1; 7.3 mm AP, 3.5 mm ML). Only certain recording sites were successfully placed in V1. To evoke visual responses in the cortex, a white light-emitting diode (LED) was placed in front of the right eye (contralateral to the recording site) of the rat and a flash of 100 ms was automatically delivered every 4 to 5 s (random delay).

Synchronous activity recording using WAG rat model

Spontaneous epileptic activity were recorded simultaneously using graphene SGFET probes and black platinum MEAs placed side-by-side and covering different areas of the cerebral cortex (S1, M1) in anesthetized WAG rats.

Animals and surgical procedure for auditory evoked field potential recording

Auditory evoked potential recordings were performed in adult male rats (OFA, Charles Rivers). Animals were housed at 24ºC, 22 Pa, in a 12-h light/dark cycle in cages with free access to food and water. All experimental procedures were performed in accordance with the recommendations of the European Community Council and French legislation for care and use of laboratory animals. The protocols have been approved by the Grenoble ethical committee (ComEth) and authorized by the French ministry (number 04815.02). Animals were anesthetized initially with 4% isoflurane induction in an inlet box (Vetflurane 2 L/min, 1.8 L air + 0.2 L O_2) and then with an intraperitoneal injection of ketamine - xylazine (ketamine 100 mg/kg : Imalgene 0.9 ml; xylazine 5 mg/kg : Rompun 2% 0.1 ml). Additional half doses were provided when necessary in order to suppress hind paw reflex movements. Temperature was monitored with a heating pad coupled to a rectal thermometer to maintain an average rectal temperature of 36 °C. The rat was placed in a Narishige stereotaxic frame with ear bars to maintain the head horizontal and fixed. A skin incision was made from between the eyes to the neck with a sterile scalpel. The skin and muscles of the left cheek were reflected with pliers and scissors to perform a wide craniotomy to expose a large part of the left hemisphere. The craniotomy ran from 2 to 7 mm posterior to bregma and from 1 to 5 mm laterally down to about 5 mm ventrally to expose the left dorsal and part of the lateral aspect of the brain down to the auditory cortex. The dura was removed and transistor arrays were placed on the surface of the cortex. Rats were then exposed to a series of 8kHz pure tones (100-ms duration with 3-ms rise and 30-ms fall times) delivered in a free field condition by a CED Power 1401 DAQ through an amplified speaker (M-Audio BX5). Data were acquired by the same CED Power 1401 controlled by Spike2 v7 software. At the end of the recording, animals were sacrificed with a letal intracardiac injection of pentobarbital (Dolethal 1 ml/kg, Vetoquinol).

Acknowledgments:This work has been funded by the European Union's Horizon 2020 research and innovation programme under grant agreement No 696656 (Graphene Flagship).The ICN2 team is supported by the Severo Ochoa program from Spanish MINECO (Grant No. SEV-2013-0295), and by the CERCA Programme / Generalitat de Catalunya. C.H. received funding from the P-SPHERE COFUND - Horizon 2020 Marie Sklodowska-Curie Actions (Grant Agreement No 665919). MVSV received also funding from BFU2014-52467-R from MINECO. This work has made use of the Spanish ICTS Network MICRONANOFABS partially supported by MINECO and also the ICTS NANBIOSIS, more specifically the Micro-Nano Technology Unit of the CIBER in Bioengineering, Biomaterials &

Nanomedicine (CIBER-BBN) at the IMB-CNM. We thank M. Ruiperez-Alonso for her contribution to the figures and C. Gonzalez-Liencres for editing assistance.

References

[1] M. Velliste, S. Perel, M. C. Spalding, A. S. Whitford, A. B. Schwartz, *Nat. Lett.* **2008**, *453*, 1098.

[2] W. J. Marks, *Curr. Treat. Options Neurol.* **2005**, *7*, 237.

[3] H. S. Mayberg, A. M. Lozano, V. Voon, H. E. Mcneely, D. Seminowicz, C. Hamani, J. M. Schwalb, S. H. Kennedy, *Neuron* **2005**, *45*, 651.

[4] R. Van Den Brand, K. Bartholdi, M. Huerlimann, L. Friedli, I. Vollenweider, P. Musienko, G. Courtine, *Science* **2012**, *336*, 1182.

[5] S. R. Soekadar, N. Birbaumer, M. W. Slutzky, L. G. Cohen, *Neurobiol. Dis.* **2015**, *83*, 172.

[6] N. B. Langhals, D. R. Kipke, *IEEE EEMBS* **2009**, 2066.

[7] E. M. Maynard, C. T. Nordhausen, R. A. Normann, *Electroencephalogr. Clin. Neurophysiol.* **1997**, *102*, 228.

[8] M. E. J. Obien, K. Deligkaris, T. Bullmann, D. J. Bakkum, *Front. Neurosci.* **2015**, *8*, 1.

[9] D. Khodagholy, J. N. Gelinas, Z. Zhao, M. Yeh, M. Long, J. D. Greenlee, W. Doyle, O. Devinsky, G. Buzsáki, *Sci. Adv.* **2016**, *2*.

[10] M. E. J. Obien, K. Deligkaris, T. Bullmann, D. J. Bakkum, U. Frey, *Front. Neurosci.* **2015**, *8*, 423.

[11] E. F. Chang, *Neuron* **2015**, *86*, 68.

[12] J. Viventi, D. Kim, L. Vigeland, E. S. Frechette, J. A. Blanco, Y. Kim, A. E. Avrin, V. R. Tiruvadi, S. Hwang, A. C. Vanleer, D. F. Wulsin, K. Davis, C. E. Gelber, L. Palmer, J. Van Der Spiegel, J. Wu, J. Xiao, Y. Huang, D. Contreras, J. A. Rogers, B. Litt, *Nat. Neurosci.* **2011**, *14*, 1599.

[13] J. Jeong, G. Shin, S. Il Park, K. J. Yu, L. Xu, J. A. Rogers, *Neuron* **2015**, *86*, 175.

[14] C. Hassler, T. Boretius, T. Stieglitz, *J Polym Sci Part B Polym Phys* **2011**, *49*, 18.

[15] S. Adam, E. H. Hwang, V. M. Galitski, S. Das Sarma, *PNAS* **2007**, *104*, 18392.

[16] L. H. Hess, M. Seifert, J. A. Garrido, *Proc. IEEE* **2013**, *101*, 1780.

[17] L. H. Hess, M. Jansen, V. Maybeck, M. V. Hauf, M. Seifert, M. Stutzmann, I. D. Sharp, A. Offenhäusser, J. A. Garrido, *Adv. Mater.* **2011**, *23*, 5045.

[18] B. M. Blaschke, N. Tort-Colet, A. Guimerà-Brunet, J. Weinert, L. Rousseau, A. Heimann, S. Drieschner, O. Kempski, R. Villa, M. V Sanchez-Vives, J. A. Garrido, *2D Mater.* **2017**, *4*, 25040.

[19] A. Fabbro, D. Scaini, V. León, E. Vázquez, G. Cellot, G. Privitera, L. Lombardi, F. Torrisi, F. Tomarchio, F. Bonaccorso, S. Bosi, A. C. Ferrari, L. Ballerini, M. Prato, *ACS Nano* **2016**, *10*, 615.

[20] L. Banszerus, M. Schmitz, S. Engels, J. Dauber, M. Oellers, F. Haupt, K. Watanabe, T. Taniguchi, B. Beschoten, C. Stampfer, *Sci. Adv.* **2015**, *1*, e1500222.

[21] T. C. Cristarella, A. J. Chinderle, J. Hui, J. Rodríguez-López, *Langmuir* **2015**, *31*, 3999.

[22] D. Kuzum, H. Takano, E. Shim, J. C. Reed, H. Juul, A. G. Richardson, J. de Vries, H. Bink, M. A. Dichter, T. H. Lucas, D. A. Coulter, E. Cubukcu, B. Litt, *Nat. Commun.* **2014**, *5*, 5259.

[23] D. Khodagholy, T. Doublet, M. Gurfinkel, P. Quilichini, E. Ismailova, P. Leleux, T. Herve, S. Sanaur, C. Bernard, G. G. Malliaras, *Adv. Mater.* **2011**, *23*, H268.

[24] Y. Xu, J. Liu, *Small* **2016**, *12*, 1400.

[25] D.-W. Park, A. A. Schendel, S. Mikael, S. K. Brodnick, T. J. Richner, J. P. Ness, M. R. Hayat, F. Atry, S. T. Frye, R. Pashaie, S. Thongpang, Z. Ma, J. C. Williams, *Nat. Commun.* **2014**, *5*, 5258.

[26] P. Ledochowitsch, E. Olivero, T. Blanche, M. M. Maharbiz, In *2011 Annual International Conference of the IEEE Engineering in Medicine and Biology Society*; IEEE, 2011; pp. 2937–2940.

[27] X. Guo, X. Liu, F. Lin, H. Li, Y. Fan, N. Zhang, *Sci. Rep.* **2015**, *5*, 10569.

[28] D. Khodagholy, T. Doublet, P. Quilichini, M. Gurfinkel, P. Leleux, A. Ghestem, E. Ismailova, T. Hervé, S. Sanaur, C. Bernard, G. G. Malliaras, *Nat. Commun.* **2013**, *4*, 1575.

[29] P. Bergveld, *IEEE Trans. Biomed. Eng.* **1970**, *17*, 70.

[30] X. Du, H. Guo, Y. Jin, Q. Jin, J. Zhao, *Electroanalysis* **2015**, *27*, 2760.

[31] M. Dankerl, M. V. Hauf, A. Lippert, L. H. Hess, S. Birner, I. D. Sharp, A. Mahmood, P. Mallet, J.-Y. Veuillen, M. Stutzmann, J. A. Garrido, *Adv. Funct. Mater.* **2010**, *20*, 3117.

[32] A. T. Valota, I. A. Kinloch, K. S. Novoselov, C. Casiraghi, A. Eckmann, E. W. Hill, R. A. W. Dryfe, *ACS Nano* **2011**, *5*, 8809.

[33] J. Xia, F. Chen, J. Li, N. Tao, *Nat. Nanotechnol.* **2009**, *4*, 505.

[34] A. Pirkle, J. Chan, A. Venugopal, D. Hinojos, C. W. Magnuson, S. McDonnell, L. Colombo, E. M. Vogel, R. S. Ruoff, R. M. Wallace, *Appl. Phys. Lett.* **2011**, *99*, 122108.

[35] B. Mailly-Giacchetti, A. Hsu, H. Wang, V. Vinciguerra, F. Pappalardo, L. Occhipinti, E. Guidetti, S. Coffa, J. Kong, T. Palacios, *J. Appl. Phys.* **2013**, *114*, 84505.

[36] M. H. Lee, B. J. Kim, K. H. Lee, I.-S. Shin, W. Huh, J. H. Cho, M. S. Kang, *Nanoscale* **2015**, *7*, 7540.

[37] C. Mackin, L. H. Hess, A. Hsu, Y. Song, J. Kong, J. A. Garrido, T. Palacios, *IEEE Trans. Electron Devices* **2014**, *61*, 3971.

[38] E. H. Hwang, S. Adam, S. Das Sarma, *Phys. Rev. Lett.* **2007**, *98*, 186806.

[39] L. Wang, I. Meric, P. Y. Huang, Q. Gao, Y. Gao, H. Tran, T. Taniguchi, K. Watanabe, L. M. Campos, D. A. Muller, J. Guo, P. Kim, J. Hone, K. L. Shepard, C. R. Dean, *Science* **2013**, *342*, 614.

[40] M. Nesladek, A. Bogdan, W. Deferme, N. Tranchant, P. Bergonzo, *Diam. Relat. Mater.* **2008**, *17*, 1235.

[41] E. C. H. Kyle, S. W. Kaun, P. G. Burke, F. Wu, Y.-R. Wu, J. S. Speck, *J. Appl. Phys.* **2014**, *115*, 193702.

[42] A. M. Goldman, *Annu. Rev. Mater. Res.* **2014**, *44*, 45.

[43] T. Fujimoto, K. Awaga, Y. Miyoshi, H. Yoshikawa, M. M. Matsushita, K. Awaga, P. Chen, L. Li, R. M. Owens, C. Liu, S. T. Nguyen, R. S. Ruoff, A. Fujiwara, T. Kariyado, H. Aoki, Y. Kubozono, X.-L. Qi, C.-X. Liu, S.-C. Zhang, Q. K. Xue, *Phys. Chem. Chem. Phys.* **2013**, *15*, 8983.

[44] B. M. Blaschke, M. Lottner, S. Drieschner, A. B. Calia, K. Stoiber, L. Rousseau, G. Lissourges, J. A. Garrido, *2D Mater.* **2016**, *3*, 25007.

[45] S. Bae, H. Kim, Y. Lee, X. Xu, J.-S. Park, Y. Zheng, J. Balakrishnan, T. Lei, H. Ri Kim, Y. Il Song, Y.-J. Kim, K. S. Kim, B. ?zyilmaz, J.-H. Ahn, B. H. Hong, S. Iijima, *Nat. Nanotechnol.* **2010**, *5*, 574.

[46] X. Wu, G. Zhong, L. D'Arsié, H. Sugime, S. Esconjauregui, A. W. Robertson, J. Robertson, *Sci. Rep.* **2016**, *6*, 21152.

[47] T. Kobayashi, M. Bando, N. Kimura, K. Shimizu, K. Kadono, N. Umezu, K. Miyahara, S. Hayazaki, S. Nagai, Y. Mizuguchi, Y. Murakami, D. Hobara, *Appl. Phys. Lett.* **2013**, *102*, 23112.

[48] J. Kang, D. Shin, S. Bae, B. H. Hong, D. Shin, B. H. Hong, S. J. Chae, X.-S. Li, A. Benayad, D. D. Loc., F. Gunes, Y. H. Lee, J.-Y. Choi, Z. F. Liu, L. M. Peng, C. A. Richter, Y. P. Chen, *Nanoscale* **2012**, *4*, 5527.

[49] M. Ruiz-Mejias, L. Ciria-Suarez, M. Mattia, M. V. Sanchez-Vives, *J. Neurophysiol.* **2011**, *106*, 2910.

[50] R. Reig, M. V. Sanchez-Vives, A. Duque, Y. Yu, D. McCormick, *PLoS One* **2007**, *2*, e670.

[51] A. Suarez-Perez, G. Gabriel, B. Rebollo, X. Illa, A. Guimera-Brunet, J. Hernandez-Ferrer, M. T. Martínez, R. Villa, M. V. Sanchez-Vives, *Adv. Healthc. Mater.*

[52] W. O. Renier, A. M. L. Coenen, *Neurosci. Res. Commun.* **2000**, *26*, 181.

[53] A. M. L. Coenen, E. L. J. M. van Luijtelaar, *Behav. Genet.* **2003**, *33*, 635.

[54] X. Du, L. Wu, J. Cheng, S. Huang, Q. Cai, Q. Jin, J. Zhao, *J. Biol. Phys.* **2015**, *41*, 339.

[55] D. Khodagholy, J. Rivnay, M. Sessolo, M. Gurfinkel, P. Leleux, L. H. Jimison, E. Stavrinidou, T. Herve, S. Sanaur, R. M. Owens, G. G. Malliaras, *Nat. Commun.* **2013**, *4*, 1575.

[56] A. A. Balandin, *Nat Nano* **2013**, *8*, 549.

[57] A. N. Pal, S. Ghatak, V. Kochat, E. S. Sneha, A. Sampathkumar, S. Raghavan, A. Ghosh, *ACS Nano* **2011**, *5*, 2075.

[58] B. Pellegrini, P. Marconcini, M. Macucci, G. Fiori, G. Basso, *J. Stat. Mech. Theory Exp.* **2016**, *2016*, 54017.

[59] M. A. Stolyarov, S. L. Rumyantsev, M. Shur, A. A. Balandin, In *2015 Fourth Berkeley Symposium on Energy Efficient Electronic Systems (E3S)*; IEEE, 2015; pp. 1–2.

[60] P. Karnatak, T. P. Sai, S. Goswami, S. Ghatak, S. Kaushal, A. Ghosh, *Nat. Commun.* **2016**, *7*.

[61] A. Allain, J. Kang, K. Banerjee, A. Kis, *Nat Mater* **2015**, *14*, 1195.

[62] M. K. Blees, A. W. Barnard, P. A. Rose, S. P. Roberts, K. L. Mcgill, P. Y. Huang, A. R. Ruyack, J. W. Kevek, B. Kobrin, D. A. Muller, P. L. Mceuen, *Nat. Lett.* **2015**, *524*, 204.

[63] J. Liu, T.-M. Fu, Z. Cheng, G. Hong, T. Zhou, L. Jin, M. Duvvuri, Z. Jiang, P. Kruskal, C. Xie, Z. Suo, Y. Fang, C. M. Lieber, *Nat Nano* **2015**, *10*, 629.

[64] X. Y. Wei, G. Ullah, X. Steven, J. Schiff, *J. Neurosci.* **2014**, *34*, 11733.

[65] A. B. Schwartz, X. T. Cui, D. J. Weber, D. W. Moran, *Neuron* **2006**, *52*, 205.

[66] S. Ahn, K. Kim, S. C. Jun, *Front. Hum. Neurosci.* **2015**, *9*, 716.

[67] Yijun Wang, Xiaorong Gao, Bo Hong, Chuan Jia, Shangkai Gao, *IEEE Eng. Med. Biol. Mag.* **2008**, *27*, 64.

[68] L. Muller, L. S. Hamilton, E. Edwards, K. E. Bouchard, E. F. Chang, *J. Neural Eng.* **2016**, *13*, 56013.

[69] K. J. Miller, K. E. Weaver, J. G. Ojemann, *Proc. Natl. Acad. Sci. U. S. A.* **2009**, *106*, 12174.

[70] T. J. Abel, A. E. Rhone, K. V Nourski, M. A. Granner, H. Oya, T. D. Griffiths, D. T. Tranel, H. Kawasaki, M. A. Howard, III, *Physiol. Meas.* **2014**, *35*, 323.

[71] B. Zhang, W. H. Lee, R. Piner, I. Kholmanov, Y. Wu, H. Li, H. Ji, R. S. Ruoff, *ACS Nano* **2012**, *6*, 2471.

[72] J. D. Yeager, D. J. Phillips, D. M. Rector, D. F. Bahr, *J. Neurosci. Methods* **2008**, *173*, 279.

[73] N. Lago, D. Ceballos, F. J Rodríguez, T. Stieglitz, X. Navarro, *Biomaterials* **2005**, *26*, 2021.

[74] K. Nagashio, T. Nishimura, K. Kita, A. Toriumi, *Appl. Phys. Lett.* **2010**, *97*, 143514.

[75] A. Venugopal, L. Colombo, E. M. Vogel, *Appl. Phys. Lett.* **2010**, *96*, 13512.

[76] M. Mukovski, S. Chauvette, I. Timofeev, M. Volgushev, *Cereb. Cortex* **2007**, *17*, 400.

[77] M. Mattia, M. V. Sanchez-Vives, *Cogn. Neurodyn.* **2012**, *6*, 239.